INTERNATIONAL ATOMIC ENERGY AGENCY
UNITED NATIONS EDUCATIONAL, SCIENTIFIC AND CULTURAL ORGANIZATION
INTERNATIONAL CENTRE FOR THEORETICAL PHYSICS
I.C.T.P., P.O. BOX 586, 34100 TRIESTE, ITALY, CABLE: CENTRATOM TRIESTE

H4-SMR 393/34

SPRING COLLEGE ON PLASMA PHYSICS

15 May - 9 June 1989

GENERATION OF DENSITY CAVITIONS IN LASER PRODUCED PLASMAS

H. C. Pant

Laser Division
Bhabha Atomic Research Centre
Bombay - 400085
India

GENERATION OF DENSITY CAVITONS IN LASER PRODUCED PLASMAS

H.C.Pant and S.Sharma

Laser division Bhabha Atomic Research Centre
Bombay - 400085 India

ABSTRACT

Density Profile modification and generation of density cavitons in laser-produced plasmas due to ponderomotive force is discussed. Earlier important theoretical work in this field is reviewed. Experimental evidence of self consistant electric field and profile modification has been presented in a chronological sequence. Some recent experimental results demonstrating caviton formation by x-ray imaging of laser produced plasma from solid targets, are also presented.

1. INTRODUCTION.

A very exciting field of experimental physics dealing with interaction of intense electromagnetic field with plasma has emerged in past three decades, with the development of high power lasers. Needless to say, there are many implications of rapid deposition of a large amount of electromagnetic energy in a plasma, of which laser-fusion is most important. Basic physics wise also, this field provides several exciting possibilities, specially when the plasma is produced by irradiating a solid target by an intense laser beam. Strong or weak density gradient plasmas (depending on the laser pulse duration) are formed along the target normal at the onset of the laser pulse. The remaining part of the laser energy then interacts with this expanding

plasma of spatially varying density, temperature and velocity. A number of laser-plasma interaction processes like stimulated Brillouin scattering, stimulated Raman scattering, two plasmon decay instability, parametric decay instability and resonance mode conversion take place in this plasma. All of them have been studied in reasonable details theoretically and experimentally. At high laser irradiances low atomic number plasma becomes fairly collisionless and the laser radiation can reach the critical density (where local plasma frequency is equal to the laser radiation frequency) nearly unattenuated by the subdense high temperature corona. Onset of this process take place nearly at laser intensities suitable for applications like laser fusion (10^{14} - 10^{15} W/cm^2). One of the most important phenomenon associated here is the modification of the plasma density gradient or profile. The profile modification takes place due to intense electric field of the swelled electromagnetic radiation near the critical density. These phenomena are discussed in next two sections. Profile modification may manifest in several forms. It could be a simple steepening of the density gradient or appearance of density depressions (cavitons). Such cavity type structures and associated self consistant electric fields have been shown to exhibit solitonic behaviour.

From laser-fusion view point, such profile modification bears important implications. Laser absorption rate remains unmodified provided the density scale length is much larger than the wavelength of the incident laser light and situation can be treated linearly[1]. However, the linear approximation breaks down even for relatively weak laser intensities. The resonant plasma wave (mode converted) field reaches large amplitudes and corresponding ponderomotive pressure leads to density modulations which modify the plasma wave coupling[1].

2.RADIATION PROPAGATION AND FIELD STRUCTURES.

As described earlier the laser driven plasma from solid targets is inhomogeneous. Typical density profile is shown in Fig.1. In the lowest order approximation the plasma dielectric constant ϵ depends on the electron density n according to

$$\epsilon = 1 - \frac{\omega_p^2}{\omega_o^2} = 1 - \frac{n}{n_c} \qquad (1)$$

where ω_p,ω_o,n and n_c are plasma frequency, laser radiation frequency, plasma electron density and critical electron density respectively. In the plasma, Maxwell's equations are

$$C\,\nabla\times E = -\frac{\partial B}{\partial t}\,, \quad C\,\nabla\times B = \epsilon\,\frac{\partial E}{\partial t} \qquad (2)$$

where symbols have their usual meaning. Considering the electromagnetic wave

$$E = E\,\exp\{i(\omega_o t - k r)\}\,; \quad B = B\exp\{i(\omega_o t - k r)\} \qquad (3)$$

the propagation equations are

$$\nabla^2 E + \epsilon\,\frac{\omega_o^2}{c^2}\,E - \nabla(\nabla\cdot E) = 0 \qquad (4)$$

$$\nabla^2 B + \epsilon\,\frac{\omega_o^2}{c^2}\,B + \frac{1}{\epsilon}\,(\nabla E)\times\nabla\times B = 0 \qquad (5)$$

For simplicity consider a linear density profile like $n=n_c(1+x/L)$; such that at x=0, $n=n_c$ and x=-L, n=0.

A plane linearly polarized electromagnetic wave is assumed to come from the vacuum side with an angle of incidence θ. When the electric field of the wave is perpendicular to the plane of incidence

(s-polarization), one gets standing waves. The turning (reflection) point for the wave is such that $n=n_c\cos^2\theta$. The curve is described by an Airy function[2], Fig.2. However, the situation is different when the electric field is in the plane of incidence (p-polarization). Now there exists a longitudinal (along the density gradient) electric field component also. The field is completely longitudinal at the turning point. The magnetic field of the wave satisfies the differential equation[2]

$$\frac{d^2B}{dx^2} - \frac{1}{x}\,\frac{dB}{dx} + \frac{\omega_o^2}{c^2}\left(\frac{x}{L} - \sin^2\theta\right)B = 0 \qquad (6)$$

under this condition of irradiation by electromagnetic wave, high amplitude oscillations are resonantly excited at the critical density (resonance point). Since the turning point of the wave is away (towards lower plasma density side) from the critical density, this effect takes place if and only if the electric field has a component along the plasma density gradient at the critical density. Such a driving field results from tunneling of the longitudinal component across the electron density gradient[2] as shown in Fig.3. If the driver electric field is E_d (due to tunneling), self consistant electric field in the plasma is given by[3]

$$E = \frac{\omega_p^2(x)\;E_d}{\omega_o^2 - \omega_p^2(x) + i\,\nu_{ei}\,\omega_o} \qquad (7)$$

ν_{ei} is electron-ion collision frequency. Resonance at the critical density ($\omega_o=\omega_p$) can be seen. It should be noted that for an angle of incidence θ equal to zero, the turning point is at the critical density. However, the field structures are described in a way similar to s-polarization case and no plasma oscillations are excited at the critical density.

There is an important point, which must be borne in mind here. The incident electromagnetic field is experiencing an increasing electron density or a decreasing dielectric constant (refractive

index). The field intensity ($E^2 + H^2$) increases as the wave travels up the plasma density gradient. The dielectric increase of ($E^2 + H^2$) value for perpendicular incidence is given by[4]

$$E^2 + H^2 = E_v^2 \left(\frac{1}{|n|} + |n| \right) \qquad (8)$$

where E_v is the vacuum electric field and n is refractive index. Here absorption of the electromagnetic radiation in the plasma has been disregarded. Such a field swelling causes forces in the plasma. Forces arising due to electric field of the radiation or electrostatic waves (produced due to resonance mode conversion) are described in the next section.

3.PONDEROMOTIVE FORCE.

It might be considered rather odd that an oscillatory electric field can produce a time averaged net force on matter. This fact arises purely because the amplitude of the electric field varies spatially. To illustrate this we take a simple example of a particle of mass m (this could be an electron) moving in x direction under the influence of an oscillatory force(an electric field in case of an electron). The equation of motion is

$$m \frac{d^2x}{dt^2} = F(x) \qquad (9)$$

F=eE for an electron in a field E, It can be expanded by x being average position of the particle over an oscillation

$$x = X + \alpha \quad \text{and} \quad F(x) = F(X) + \alpha \frac{dF}{dx} \qquad (10)$$

The two equations of motion are

$$m \frac{d^2\alpha}{dt^2} = F(x) \sin \omega t \qquad (11)$$

Solution being

$$\alpha = - \frac{F(x)}{m\omega^2} \sin \omega t \qquad (12)$$

and

$$m \frac{d^2x}{dt^2} = \frac{dF}{dx} \langle \alpha \sin \omega t \rangle \qquad (13)$$

This equation describes the slowly varying evolution of X(t), the average position of the particle, < > sign means a time average over a period of the oscillating force from equations 12 and 13.

$$m \frac{d^2x}{dt^2} = - \frac{d}{dx} \left(\frac{F^2}{4m\omega^2} \right) = - \frac{d}{dx} \left(\frac{1}{2} m \langle \dot{\alpha}^2 \rangle \right) \qquad (14)$$

$$F_p = \frac{d}{dx} \left(F^2/4\pi\omega^2 \right) \qquad (15)$$

Thus average position of the particle is seen to move in a quasipotential $\phi = (F^2/4\pi\omega^2)$

From electric field view, ponderomotive force per unit volume[5]

$$F_p = \frac{e^2 n_o}{4m} \nabla \frac{|E_s(x)|^2}{\omega_o^2} \quad \text{or} \quad F_p = \frac{\epsilon^2 n}{2m} \frac{\nabla \langle E^2 \rangle}{\omega_o^2} \qquad (16)$$

where

$$E = \frac{1}{2} E_s(x,t) e^{-i\omega_o t} + c.c \qquad (17)$$

and n_o, m and e are electron density mass and charge respectively. ω_o^{-1} is the rapid time scale and E(x,t) accounts for both the full spatial

and slow time scale variation.

This force is essentially due to gradient of the pressure exerted by the rapid oscillatory motion of the electrons in the electric field of the electromagnetic radiation (laser) and is only part of the force exerted on the plasma by the field.

The complete expression for the pressure (Tensor) P_r giving rise to the field is

$$\underline{\underline{P_r}} = \frac{1}{8\pi} \langle E^2 + H^2 \rangle \underline{\underline{I}} - \frac{1}{4\pi} \langle \underline{E}\underline{E} + \underline{H}\underline{H} \rangle + mn\langle \dot{x}\dot{x} \rangle \qquad (18)$$

$$mn \langle \dot{x}\dot{x} \rangle = \frac{ne^2}{m\omega^2} \langle \underline{E}\,\underline{E} \rangle = \frac{1-\epsilon}{4\pi} \langle \underline{E}\,\underline{E} \rangle \qquad (19)$$

where ϵ is dielectric constant. Thus we can write[6]

$$\underline{\underline{P_r}} = \frac{1}{8\pi} \langle E^2 + H^2 \rangle \underline{\underline{I}} - \frac{1}{4\pi} \langle \epsilon \underline{E}\,\underline{E} + \underline{H}\,\underline{H} \rangle \qquad (20)$$

From this pressure term one can derive F_p. The first term does not contain plasma denstiy explicity. However, in a plasma $H=\epsilon E$, where ϵ depends on electron density. Thus the plasma density term is included in it[7].

The ponderomotive force term applies to both electromagnetic and longitudinal electron plasma waves. The force acts directly on the electrons. However, due to change separation, it eventually acts on the plasma as a whole. The main point is that one has to distinguish between high frequency phenomenon in which ions may be considered as motionless neutralizing background and low frequency processes in which both species move together. In the two cases the electron density profile has to be calculated consistantly with the field, the ponderomotive force providing the coupling.

Implications of radiation pressure (ponderomative pressure) on the hydrodynamics of laser-produced plasmas are important. In the next section we would discuss some of the issues and focus primarily on profile modification problem.

4. THEORY AND SIMULATIONS.

4.1 Max and Mckee[8] have shown from hydrodynamical considerations that profound density profile modifications are possible in the corona of laser produced plasmas from solid target, when radiation pressure (ponderomotive) effects are included. Plasmas, which enter critical density region from overdense (ablation) region supersonically, exhibit compressional density profiles. On the other hand plasmas entering the critical region subsonically exhibit a sharp density step (steepend profile). In this analysis jump conditions in a frame moving with the critical density layer can be written as following (see Fig.4).

$$\rho_1 v_1 = \rho_2 v_2 \qquad (21)$$

$$p_1 + \rho_1 v_1^2 = p_2 + \rho_2 v_2^2 + P_r \qquad (22)$$

ρ , p , v and P_r are density, plasma kinetic pressure, plasma flow velocity and radiation pressure respectively. 1 and 2 refer to two regions (Fig.4). P_r is $(E^2 + H^2)/ 8\pi$ for a normally incident radiation (laser) on a one dimensional plasma. The radiation propagation is taken along the density gradient of the flowing plasma. The equation 21 and 22 are solved. The result being

$$\frac{\rho_1}{\rho_2} = \frac{M_2}{M_1} = \frac{1 + M_1^2 - (P_r/\rho_1 c_1^2) \pm \left[\left(1 + M_1^2 - P_r/\rho_1 c_1^2\right)^2 - 4 M_1^2 \right]^{1/2}}{2 M_1^2} \qquad (23)$$

where

$$M_1 = v_1 / \sqrt{p_1/\rho_1} = \frac{v_1}{c_1} \; , \; M_2 = v_2 / \sqrt{p_2/\rho_2} = \frac{v_2}{c_2} \qquad (24)$$

$$M_1 = \frac{v_1}{\sqrt{p_1/\rho_1}} = \frac{v_1}{c_L} \quad ; \quad M_2 = \frac{v_2}{\sqrt{p_2/\rho_2}} = \frac{v_2}{c_2} \qquad (24)$$

for isothermal condition in the neighbourhood of the jump

$$\sqrt{\frac{p_1}{\rho_1}} = \sqrt{\frac{p_2}{\rho_2}} \quad \text{or} \quad c_1 = c_2 \qquad (25)$$

for real solutions,

$$M_L \geq M_R \equiv \sqrt{1 + p_r/\rho_L c_1^2} \qquad (26)$$

$$M_1 \leq M_D \equiv \sqrt{1 - p_r/\rho_1 c_1^2} \qquad (27)$$

Max and Mckee[8] identify these conditions with two types of flow (defined by the type of fronts they produce near the critical density). They are called R and D fronts [Fig.5(a,b)] and identified with equations 26 and 27 respectively. Since the velocity does not change its sign across the critical surface implies $P_r < \rho_1 c_1^2$ meaning $M_D > 0$.

One can see that R fronts represent compressions ($\rho_1 < \rho_2$; $M_1 > M_2$) whereas D fronts indicate rarefactions ($\rho_1 > \rho_2$; $M_1 < M_2$); Thus, D front represents a density step in which the plasma flows subsonically into the critical surface and then accelerates to supersonic velocity afterwards. The total pressure ($p_2+\rho_2 v_2^2+P_r$) is balanced by thermal pressure p_1 (Fig. 5a).

In case of R fronts plasma flows supersonically into the critical region. It's pressure $\rho_1 v_1^2$ must balance the total pressure ($p_2+\rho_2 v_2^2+P_r$). Due to radiation pressure in the counterflow direction, the matter piles up in the critical density region (Fig.5b). However, such fronts suffer from instability due to perturbations which may lead to lowering of peak density at the front slightly below critical.

It is suggested[8] that a shock plus D front (Fig.5c) would be more stable as a simple shock can stand upstream of the critical surface and can bring down the flow speed from supersonic to subsonic. Because of the shock the flow at the critical density would now become subsonic and allow D front condition to exist. Since the critical density now exists far below on the d front step, a small perturbation to the peak density at the front will not affect the critical surface position. Needless to say such compressional structures require dissipation in order to exist. Such a dissipation may be provided by plasma turbulence. Energy transport and laser absorption may be significantly affected due to such a turbulence[8].

4.2. Several simulation experiments have also been made to understand density profile modification due to ponderomotive forces[9-12]. Lee et al[10] have predicted density steepening at the critical layer in one dimensional plasmas produced from planar targets, irradiated obliquely by s-polarized light. However, for long pulse experiments (which are of relevance in ablative compression studies), even initially one dimensional flow diverges, necessitating the use of spherical geometry. Virmont et al[11] have studied such a situation in their simulations. Fluid equations of the plasma are

$$\frac{\partial \rho}{\partial t} + \frac{1}{r^2}\frac{\partial}{\partial r}(\rho v r^2) = 0 \qquad (28)$$

$$\frac{\partial \rho v}{\partial t} + \rho v \frac{\partial v}{\partial r} + \frac{\partial p}{\partial r} = -\frac{1}{8\pi}\frac{\rho}{\rho_c}\frac{\partial E^2}{\partial r} \qquad (29)$$

.The field equation is

$$\left[\frac{\partial}{\partial r^2} + \frac{2}{r}\frac{\partial}{\partial r} + k_0^2\left(1 - \frac{\rho}{\rho_c}\right)\right] E = 0 \qquad (30)$$

where the terms have their usual meaning. Radiation absorption has been completely ignored here. This means the gradient of E^2 arises purely due to propagation effects and not from absorption. Electric fields in the simulations are calculated for various values of simulation zone thicknesses and using WKB approximation as well as

wave equation. Fig.6a shows the density profiles obtained with a target sphere of 100 μm, at various times. An overdense bump formation can clearly be seen. The top and external front of the bump are stationary in the frame of critical surface. Fig.6b shows the density and the velocity profile in the moving frame for a given time (440 psec). One can see that a subsonic dip in the velocity profile corresponds to the overdense bump in the density profile in presence of a preformed plasma with an initial density profile (formed by a laser prepulse), profiles similar to 6a are obtained (see Fig.6c).

4.3.

Morales and Lee[12] have dealt with the problem by specifically considering electrostatic resonance at the critical point due to evanescent radiation. For this reason they have considered pump as a long wavelength wave. Such a situation is more realistic and is realized in laser fusion experiments where resonance mode conversion is important. There are also other laboratory experiments where quasi-electrostatic field generated by large capacitor plates is used as an external pump for the plasma. This treatment describes the spatial and temporal evolution of the electric field through non linear Schrodinger equation. Density modification is obtained from the ion-acoustic wave equation with the effects of ponderomotive force included in the investigations. Considering an unmagnetized plasma slab with plasma density

$$n_0(x) = n_c \left(1 + \frac{x}{L} \right) \tag{31}$$

where x is the spatial co-ordinate, L is the gradient scale length and n_c represents the critical density (resonance point density). The space-time dependence of the total high frequency field $\mathcal{E}$ is represented in the form

$$\mathcal{E} = E(x,t)\, e^{-i\omega_0 t} + c.c. \tag{32}$$

Combining the continuity and force equations for high frequency response of the electron fluid (n_h)

$$\frac{\partial^2 n_h}{\partial t^2} - 3\bar{v}_e^2 \frac{\partial^2 n_h}{\partial x^2} - \frac{\partial}{\partial x}\left[\frac{e}{m} (n_0 + n_l)\mathcal{E} \right] = 0 \tag{33}$$

where n_l refers to the slowly varying fluctuations e, m, $v_e[=(T_e/m)^{0.5}]$ are charge mass, thermal velociy of electrons and electron temperature respectively. Using Poissons equation

$$\frac{\partial}{\partial x}(\mathcal{E} - \mathcal{E}_0) = -4\pi n_h \tag{34}$$

and assuming $\mathcal{E}_0 = E_0 e^{-i\omega t} + c.c.$

where is the vacuum driving field. One then obtains

$$\frac{2i}{\omega}\frac{\partial E}{\partial t} + \frac{3\bar{v}_e^2}{\omega^2}\frac{\partial^2 E}{\partial x^2} + \left\{ 1 - \frac{4\pi e^2}{m\omega^2}[n_0(x) + n_l] \right\} E = E_0 \tag{35}$$

taking $\partial^2 E/\partial t^2$ to be very small and hence dropping it. Slow time scale equation governing n_l is obtained by adding force equation for electrons and ion fluid combining with continuity equation, one gets (in the neighbourhood of the resonance point)

$$\frac{\partial^2 n_l}{\partial t^2} - c_s^2 \frac{\partial^2 n_l}{\partial x_2} = c_s^2 \frac{\partial}{\partial x^2}\left(\frac{|E|^2}{4\pi n_0 t} \right) \tag{36}$$

here $c_s = (T_e/M_i)^{0.5}$. It is the ion-acoustic wave equation of self consistent ponderomotive force which has been introduced as a source term.

Introducing following scalings :

$$Z = (k_D L)^{2/3}(x/L), \quad \tau = (k_D L)^{-2/3}(\omega t/2)$$

$$A = (k_D L)^{-2/3}(E/E_0), \quad k_D^{-2} = 3(\bar{v}_e/\omega)^2$$

$$N = (k_D L)^{-4/3}\left(\frac{E_0^2}{4\pi n_c t} \right)^{-1} \frac{n_l}{n_c}$$

$$P = (k_D L)^2 \left(\frac{E_0^2}{4\pi n_c t} \right)$$

$\Gamma = (k_D l)^{2/3} (\nu/\omega)$; ν : collision freq.

The new transformed equations are

$$i \frac{\partial A}{\partial \tau} + \frac{\partial^2 A}{\partial Z^2} - (Z - i\Gamma + pN) A = 1 \qquad (37)$$

$$v^2 \frac{\partial^2 N}{\partial \tau^2} - \frac{\partial^2 N}{\partial Z^2} = \frac{\partial^2 |A|^2}{\partial Z^2} \qquad (38)$$

is the dimensionless damping rate and p is a parameter which determines the strength of non-linearity. For $p > 1$ is a non-linear case where as $p << 1$ is a linear situtation. The equations 37 and 38 are a set of coupled equations which are solved to determine the self consistent field and density perturbations. The low frequency non-linear ponderomotive force provides a coupling term.

For small amplitude pumps ($p << 1$) the behavior is determined by the linear equation

$$i \frac{\partial A}{\partial \tau} + \frac{\partial^2 A}{\partial Z^2} - (Z - i\Gamma) A = 1. \qquad (39)$$

.The term $\partial^2 A / \partial Z^2$ arises due to thermal motion of the electrons, and is found to play a crucial role by producing a net convection of the electric field energy away from the resonant regions,in the direction of decreasing density. This process of convection saturation limits the electric field amplitude at the resonance point.

In the linear regime the steady state behavior of the system is given by $(\partial A/\partial \tau) = 0$

$$\frac{\partial^2 A}{\partial Z^2} - (Z - i\Gamma) A = 1. \qquad (40)$$

. The solution is

$$A(\psi) = -\pi [G_i(\psi) + i A_i(\psi)]$$

where $\psi = Z - i\Gamma$, A_i is Airy function and

$$G_i \sim (\pi \psi)^{-1} \quad \text{For } Re\ \psi >> 1$$

$$G_i \sim \pi^{-1/2} \psi^{-1/4} \cos\left(\frac{2}{3} \psi^{3/2} + \frac{\pi}{4}\right)$$

$$\text{For } Re\ \psi << -1$$

For non-linear response, initially the effects of ion inertia are neglected that is $v^2 \partial^2 N/\partial \tau^2$ term is dropped. This is appropriate if $v^2 << 1$ or if, the local group velocity of the high frequency field is small compared with the ion acoustic speed. Therefore,

$$\frac{\partial^2 N}{\partial Z^2} = -\frac{\partial^2}{\partial Z^2} |A|^2 \qquad (41)$$

. The solution is $N = -|A|^{+2}$. The equation 37 now becomes

$$i \frac{\partial A}{\partial \tau} + \frac{\partial^2 A}{\partial Z^2} - (Z - i\Gamma - p|A|^2) A = 1 \qquad (42)$$

. This is a driven non-linear Schrodinger (NLS) equation in a non-uniform plasma.

This equation is the nonlinear counterpart of linear equation, hence it describes the process of non-linear mode conversion whereby the pump field initially mode converts into a Langmuir wave near the resonance point, and in this process it alters the density profile in a self consistant manner. For large pump fields or in other words for large values of p (>0.8), density cavities or pockets begin to appear in the profile, hence, the wave functions become closer to soliton like structures (unlike Airy solutions for negligible value of p). It is worth noting here that the generation of density cavities and localized strong electric fields in a non uniform plasma do not require the amplitude of the electric field (Eo) to be very large. Value of parameter

$$p \left[= \left(\frac{\omega L}{v_e} \right)^2 \frac{E_o^2}{12 \kappa n_c T} \right]$$

can be very large experimentally (> 1) even for modest values of E_o^2.

Value of p decides the threshold for this regime. One can now discuss strong non-linear behavior first without and later with ion inertia.

The adiabatic distortion of Airy type pattern ($p \ll 1$) is strongly altered when the pump amplitude is increased beyond the $p > 1$ level. The reason for strong modification of the linear mode conversion process at these large amplitude levels is that the localised density cavities are generated in the plasma by ponderomotive force. These density cavities cause a partial reflection of the mode converted waves and also alter the efficiency of mode conversion due to the local steepening of the profile. One can see the direct effect on the mode conversion pattern by introducing a localised density cavity in the density profile. Considering the steady state equation

$$\frac{d^2 A}{d z^2} - \left[z - N(z) \right] A = 1 \qquad (43)$$

$$\text{with} \qquad N(z) = \left\{ 2.5 \, \text{Sech} \left[4(z-1) \right] \right\}^2 \qquad (44)$$

which represents a narrow density cavity in the overdense region. The effect of such a cavity is clearly seen in Fig.7 on $|A|^{+2}$. Curve a is for linear profile and b is generated when the cavity is introduced. Creation of a cavity in the density profile in the overdense side gives rise to a strong localization of the electric field. The spatial localization arises because the cavity now provides a potential well within which the Langmuir oscillations are partially trapped i.e. they are prevented from convecting down the density gradient. As the degree of trapping increases, so does the peak amplitude of the localized field. In this case the profile is not self consistant with the electric field. One can see a case of self

consistant electric field and associated density cavity for p=3, =0.2 at z=1.75 (Fig.8). It is clear that the self consistant distortion of the profile moves the resonance point deeper into the plasma and creates a sharp density at the original location of the resonance. However, now the density cavity is not bound at the two ends by the critical density and therefore Langmuir oscillations are able to leak out and convect the energy down the density gradient. Thus a steady state does not evolve. For self consistant case the localized field energy is convected down the density gradient. While moving down the gradient, the field drags the density cavity. Another density cavity is now produced because the resonance region now shifts deeper into the plasma while the pump field is still on. The cycle is repeated. Stages of evolution of electric field and density cavity at various times is shown in Fig.9.

The effect of ion inertia on the process of generating density cavities and localised self consistant fields appears via parameter

$$V = \left(\frac{4M}{3m} \right)^{1/2} \left(k_D L \right)^{-1/3} \qquad (45)$$

. Features which appear different from the case where ion inertia is neglected. are (i) the evolution of nonlinearity is slower when ion inertia is included. (ii) Ponderomotive force now produces density bump as well as a cavity. This additional feature implies that as the initial density cavity centered around near the resonance point develops, it pushes the excess density up and down the density gradient. As a result now it is possible to generate a cavity bounded by critical density. This also would mean localization of the electric field (iii) Fission of large individual cavity into subcavities. This splitting is associated with the fact that the temporary barrier created by the density bump cannot hold high frequency energy on the low density side of the gradient for a long time. After some time the energy begins to leak out on this side leaving behind a small cavity. (iv) clear indication of profile steepening in the neighbourhood of the resonance region and the shape of the density cavity is no longer mirror image of the self consistant field intensity $|A|^{+2}$. Time

evolution of these features is shown in Fig.10.

Chen and Liu[13] have determined analytically the threshold conditions for generation of N-solitons and their effects on density profile modification for long density gradient plasmas associated with relatively weak pumps, so that the wave breaking processes are ignored. In their treatment, they have also solved a driven nonlinear Schrodinger wave equation. They have considered two situations for soliton generation. In the first case the linearly transformed waves (mode conversion) are saturated by thermal convection and subsequently Landau damped much before the self consistant ion motion comes into play i.e. convection saturation time

$$t_c \simeq (k_D L)^{2/3} \omega_{pe}^{-1} \qquad (46)$$

is much less compared to the ion period

$$\omega_{pi}^{-1} = \left(\frac{M_i}{4\pi n_e e^2}\right)^{1/2} \qquad (47)$$

where L is the unmodified plasma density scale length,

$$k_D = \frac{2\pi}{\lambda_D} \quad ; \quad \lambda_D = \left(\frac{T}{4\pi n_e e^2}\right)^{1/2} \qquad (48)$$

M_i is the ion mass. Condition for N soliton generation is

$$\pi E_d L^{5/3} > N\pi \qquad (49)$$

where E_d is the evansascent driving field as mentioned earlier. Each time a soliton is generated at the resonance point, it modifies the density profile and shifts the critical density surface to new position deeper in to the plasma and slowly convects out of the resonance point. A new soliton is then generated at the shifted resonance point. The ultimate effect of these soliton generation is that the density profile is steepened with a final scale length (L_f) given by

$$L_f = \frac{1}{E_d^{3/5}} \sim \left(\frac{k_o}{P}\right)^{3/7} \qquad (50)$$

where P is the incident power and k_o is the incident propagation constant.

In the second situation, the convection saturation time of the plasma wave is long compared to the ion period (ω_{pi}^{-1}). In this case the solitons are generated during the growth phase of the plasma waves and convect down the density gradient where they are damped by interacting with hot electrons. The condition for N-soliton generation in this case is

$$\pi(N+1/2) > (PL\lambda_o)^{1/2} > \pi(N-1/2) \qquad (51)$$

The energy carried away by the solitons is finally absorbed in the plasma. The absorption co-efficient is found to be independent of temperature of the plasma, the intensity and wavelength of the incident radiation. The absorption co-efficient (a) is given by

$$a = \frac{|\phi(s)|^2}{\pi} \qquad (52)$$

where $\phi(s)$ is the resonance function and $s = (k_o L)^{1/3} \sin\theta$, θ is the angle of incidence of the radiation on the plasma.

First experimental verification of density profile modification was shown by Stenzel Wong and Kim[14]. In their experiment, S-band microwaves (f=2000 MHz, λ=15cms) were incident on a quiescent, steady state magnetic field-free plasmas produced by a dc discharge in argon at 10^{-3} Torr. These experiments demonstrated the basic signatures of resonance absorption of radiation and density perturbation. The electric field strength of the resonant plasma waves was observed to be 3 orders of magnitude larger than that of local evanascent electromagnetic field in the vicinity of the critical density region. Associated with the electrostatic waves in the resonant region a perturbation of the plasma density was observed. The perturbed density $\propto \delta n/n_c$ which varied linearly as E^2; where δn, n_c

and E represented the perturbed, the critical density and field due to electrostatic plasma waves respectively.

In their later experiments[15] Kim, Stenzel and Wong group demonstrated the role of ponderomotive forces associated with the electron plasma waves in generating density cavitons. The density cavitons trapped in the plasma wave r.f. field were mutually enhanced. The spatial and temporal behavior of the plasma wave field E and the corresponding density perturbation $\delta n/n_c$ are shown in Fig.11. The density perturbation δn and the plasma wave amplitude E grew simultaneously exponentially. The growth rate was found to vary linearly with the pump power E_0^2 of the incident rf radiation . The density perturbation established as $\delta n/n_c$. For gentle density gradients $\langle E^2 \rangle$ and δn break down into several peaks out from the resonant regions towards regions of higher and lower densities. For steeper density gradients a short wavelength ion-acoustic wave was generated inside the density cavity which propagated down the density gradient. With the generation of ion acoustic wave the plasma wave field (E^2) was found to oscillate in the density cavity with an ion-acoustic frequency. Accelerated ion fluxes were observed up and down the density profile with much stronger ion flux down the density gradient[16]. The ion-acceleration and density cavity formation was attributed to the strong non-linear low frequency ponderomotive forces of the highly localized plasma wave field amplitude. The density cavitons serve as resonant cavities for the plasma waves. The estimates of the eigenmodes for the trapped electron plasma waves in the caviton were demonstrated by Tanikawa et al[17]. In these experiments they measured the decay time constants of the trapped fields as well as the width and depth of the associated cavitons. The eigenmodes of the trapped field were calculated by assuming the density caviton to be a parabolic cavity. In addition they compared their results with numerical simulations of the Zakharov equations and also found agreement with simulations of G.J.Morales et al[12]. In ionospheric plasma experiments, small-scale cavitons embedded inside large cavitons have been successfully observed[18], Fig.12. Such a direct observation of cavitons can help in explaining a number of

nonlinear processes in the active modification of the ionosphere by high power em waves. Production of cavitons also leads to a method of remote excitation of low frequency ion acoustic waves in the ionosphere. The excitation of ion acoustic waves at frequencies much greater than the collision frequency is a manifestation of the action of the ponderomotive forces associated with the incident electromagnetic wave and/or the enhanced es waves.

In the above subsection we have mentioned the experimental demonstration of processes such as resonance absorption, density profile modification and generation of density cavitons in the interaction of microwave radiations with dc plasmas. Such plasmas happen to be steady state, low density ($\sim 10^9 - 10^{10}$ cm^{-3}) and low temperature ($\sim$ 1-2 eV) plasmas. In contrast the laser-produced plasmas are flowing plasmas with high density($10^{18} - 10^{22}$ cm^{-3})and hot ($\sim$ 1kev plasmas). Life time of these plasmas is very short $\sim$ (nano second) as they are produced by short pulsed $\sim$ (nanosecond) high intensity lasers. Absorption processes in such short lived, hot and dense plasmas are complicated by processes of x-ray emission, generation of instabilities, laser harmonics and large scale self generated magnetic fields of mega Gauss order. These absorption processes are further affected by the finite laser spot size and lateral heat transport of energy in the regions surrounding the laser focal spot. At high laser intensities ($> 10^{14}$ W /cm^2 for Nd glass laser and $> 10^{12}$ W /cm^2 for CO_2 laser) the radiation pressure becomes comparable to thermal plasma pressure. The dominant radiation pressure or the ponderomotive forces associated with high laser intensity modifies the plasma density profile drastically and leads to generation of density cavitons.

Density cavitons in laser-plasmas were demonstrated by Donaldsen and Spalding[19]. Plane carbon targets were irradiated by 75J, 50ns carbon dioxide laser at an intensity $\sim 10^{13}$ W/cm^2. Holographic interferometry and x- ray camera were employed to determine density profiles and plasma emissivity. Interferometric records were taken 25 ns after the start of the laser pulse. From the density profiles,

density cavitons with radial and axial scale lengths of 200 and 50 μm respectively were observed in the critical density region with a resolution of 50 μm. Both laser pulse and cavitons existed for times of order $10^6\ \omega_{pe}^{-1}$ and quasi-steady-state conditions were established. The ratio of the radiation to thermal pressure i.e. $E_c^2/8\pi nkT$ in these experiments was 0.16; where E_0 represented the vacuum electric field and the plasma temperature was ≈ 1.6 Kev.

Fedosejevs et al[20] observed self steepening in plasmas produced by irradiating plane aluminum targets with a 60J, 1-2 ns CO_2 laser. The aluminum targets were oriented at ≈ 20° with the laser axis. Time resolved interferogram were recorded with a spatial resolution of 15 μm. During initial irradiation stage a super critical density shelf at ≈ $5n_c$ was observed which in later stages developed upto 7 n_c. This shelf was accompanied by a steep rise of profile through the critical density. At a laser intensity ≈ 10^{14} W/cm² and plasma temperature T_e ≈ 400 eV, the ratio of radiation pressure to thermal pressure i.e $(I_L/c)/(n_c kT) = 1/2\,(v_c/v_e)^2$

was roughly 5.2. The results were in agreement with simulation results which predict an upper and lower density shelf connected by a steep rise through the critical density. In their later experiments on glass microballoons targets Fedesejevs et al[21] observed the above mentioned predictions of simulation results in their time resolved interferometric density profile measurements. The density profile consisted of an upper density shelf followed by a density caviton, a density bump at a density height of ≈ 40 n_c. The density bump was connected to a lower density shelf by a steep fall through the critical density. The caviton width and the bump thickness increased with time during the laser pulse. These structures were in agreement with shock and density step profiles predicted by Max and Mckee[8] in their hydrodynamical calculations for a supersonic plasma flow and simulation results of Virmont et al[11]. Besides the density shelves and cavitons with bumps; cratering in the critical density and large scale rippling in the subdense plasma were observed. The density scale length at the critical density was found to be a function of intensity

and flow velocities. The scaling with intensity was determined as

$$\frac{L_c}{\lambda_D} = 39.6 \left(\frac{I}{10^{13}}\right)^{-0.48} \qquad (5.3)$$

Zakharenkov et al[22] demonstrated the presence of density cavitons in the plasma profiles produced by 200-250J, 1ns, 1.06 μm Nd-glass laser. Plane aluminum targets were irradiated at intensity ≈ 10^{14} W/cm². The density profiles were drawn using interferometric and x-ray diganostics Fig.13. In the overdense region, the density steepend to ≈ $2n_c$. The cavitons ≈ 300 μm in width were observed in the critical density region at the end of the laser pulse (2-3 ns). However, in short pulsed lasers (≈ 100 ps), with intensities ≈ 10^{15} W /cm², Briand et al[23] observed transient cavitons during the laser pulse with glass microballoon targets. Cavitons ≈ 5 μm wide and ≈ 0.3 n_c deep were observed in the critical density region along with thin overdense bumps slightly above the critical density Fig.14. Experiments carried out with still shorter pulses 30 ps and higher intensities ≈ 10^{16} W /cm² have essentially shown sharp profile steepening with upper and lower density shelves[24-26]. Density scale length in the steepened region ≈ λ. Raven and Willi[26] have predicted a scaling for the density jump $\delta n/n_c \approx (I/cnkT)^{0.5} \approx I^{0.17}$ as T scales with intensity as $I^{0.66}$, where symbols have their usual meaning.

From the laser plasma experimental results described above, it is observed that in long pulsed lasers, the cavitons are produced near about the peak of the laser pulse and have long life while in short pulsed experiments the cavitons are produced or transients during the laser pulse or instead the profile is sharply steepened.

The experiments were conducted using a 1.06 μm Nd:glass laser chain which could deliver a plane polarized laser beam of 50 joules in 6 ns pulses. The diameter of the nearly diffraction limited beam was 60 mm. The laser was incident normally and focussed to 30 μm on a machined plexiglass target slab by an f/1.5 aspheric lens. X-ray emission from the plasma was recorded by a pinhole camera positioned normal to the laser beam axis. The pinhole aperture diameter of the

camera and its magnification were 11 μm and 6x respectively. Thin aluminum filters were employed for spectral discrimination.

The x-ray pictures were recorded on double emulsion type Kodak Direct Exposure Film (DEF-5). The film was developed for 6 minutes at 20^{0} C. The x-ray pictures were digitized on Joyce-Loebl SCANDIG microdensitometer connected to PDP-11/40 computer. The absolute energy density was obtained using the universal relation

$$\alpha D = a \ln (1 + b \beta I) \qquad (54)$$

established by B.L.Henke et al[27 28] for DEF films.

The electron density profiles are obtained by a variable point Abel inversion technique assuming cylindrical symmetry around the central axis of the expanding plasma. In the intensity range of our experiments the plasma attains a temperature of 680 eV[29] and is assumed to be isothermal. Data smoothening was carried out by using a Chebyshev Polynomical fit.

A representative photograph of x-ray pinhole picture of the plasma produced by 23.4 J of laser energy with an intensity of 5.4 x 10^{14} W/cm^2 is reproduced in Fig.15b. The photograph shows a narrow bright emmission region close to the target followed by a dark band and bright expanding coronal region in succession. The axial dimensions of these regions can be seen in the densitometric trace of the picture shown in Fig.16. The peak emission occurs 20 μm away from the target surface. Thereafter, corresponding to the dark region in the photographs the emission drops abruptly to a minimum at ≈ 150 μm; followed by a steep rise in emission forming a nearly 140 μm wide cavionic valley. Beyond the valley, there exists a freely expanding coronal region extending upo 1000 μm. Evolution of film energy density profiles with incident energy is shown in Figures 17 a,b,c (corresponding to photographs of 15 a,b,c). Fig.17b shows a clear appearance of a caviton at 19.6 J. The caviton becomes deeper at 23.0 J as shown in Fig.17c.

Figures 17c and 17d show respectively, the side view and the front view of the surface plots of film energy density. The arrows indicate the direction of the incoming laser beam. Fig.17c clearly depicts a profile steepening in the vicinity of the target; a deep and wide cavitonic valley, spread along the entire radial extent of the plasma and a steeply rising front on the right of the valley minimum. It should be noticed that small scale structures are present within the cavity bed and in the expanding corona. Fig.17d shows the radial features of the plasma in the target vicinity and coronal region. In addition to axial cavitons radial cavitons are also observed close to the critical regions. These radial cavitons may be formed by self modulation of a focussed laser beam into filaments due to radial ponderomotive forces associated with the high intensity of the laser beam.

An axial plasma density profile at 23.4 J is shown in Fig.18. Close to the target a density steepening with a peak density ≈ 2 n_c is observed. One can see a small caviton centered at 60 μm with a width of 50 μm and depth ≈ 0.6 n_c becoming apparent in the density plot. The large caviton is centered around 160 μm. This large caviton is 130 μm wide at the top and has an average depth of ≈ 0.8 - 0.9 n_c. Beyond the cavitonic minimum there occurs sharp rise in density forming compression front at 190 μm. The front is less than 20 μm thick and ends up in an overdense bump slightly above the critical density (1.1 n_c) at 220 μm. The overdense bump is also around 20 μm thick and seperates the cavitonic region from a long subdense coronal shelf at around 0.3 n_c. In this density prolfile we definitely expect some error due to assumption of th narrow band transmittion of the x-ray filter. However, the gross features in the relative density structure remain unaffected. Since our x-ray pictures are time integrated, it should be noticed that both laser pulse and cavitons and other features exist for long times of the order of $10^6 \omega_o^{-1}$, establishing steady state conditions. The upper density scale length L_u in the steepest region is less than 10 μm while the lower density scale length L_l in the subdense region is around 190 μm. The measurement of upper scale length in our experiments is limited by camera resolution

(11 μm). In practice it can be of the order of the incident wave length.

In this series of experiments we have observed an intensity threshold of ≈ 4 x 10^{14} with a corresponding energy of ≈ 17 J at which a small caviton is formed in the target vicinity ≈ 40 μm away. The threshold is in good agreement with the calculations of Hora (7 x 10^{14} W/cm^2) for the dominance of ponderomotive forces over the thermal forces.

The various features of our experimental profiles are in good qualitative agreement with R - front profiles predicted in the hydrodynamic calculations of Max and Mckee[8] for supersonic plasma flow and the simulation results of G.J.Morales et al[12], Virmont et al[11] analytical model of Lee et al[10].

From the above mentioned experimental results and earlier discussions we conclude that sharp density step profiles are the characteristics of steep gradient, short pulsed laser plasmas, while the formation of large cavitons appears to be a characteristic of relatively weaker gradient, long pulsed laser plasmas.

6, CONCLUSIONS.

Non-linear ponderomotive forces due to radiation pressure play a crucial role in the process of plasma heating. Absorption of pump radiation, various instabilities generated velocity distributions and energy transport in plasma; all sensitive to density gradient scale lengths. Interaction of large amplitude self consistant electric fields and ion density perturbation at high laser intensities alter these density gradients and lead to a non-linear steepening of the plasma profile through the ponderomotive force, thus, affecting the very important above mentioned processes. Profile steepening and generation of density cavitons have been demonstrated practically in all types of plasmas such as d.c. discharge, ionospheric, magnetized

and laser produced plasmas. Generation of density cavitons produce non-monotonic density profiles in a plasma. Such non-monotonic profiles consist of super-critial density shelf in the overdense region, a density pocket or a density caviton in the critical density region and a sub-dense shelf in the coronal region. These non-monotonic profiles can never be produced by thermokinetic forces alone and are the first conclusive proof of the non-linear forces operating in radiation-plasma interaction. In order that the cavitons be produced by thermokinetic forces along would require a higher temperature at greater depth in the plasma; which seems to be absurd. However, highly localized, large amplitude electron plasma waves are responsible for caviton generation by expelling the plasma from the resonance region via non-linear, low frequency ponderomative force. The ponderomotive force primarily acts on the lighter species i.e. electrons which are accelerated out of the plasma resonance. The resultant ambipolar field produced to maintain the charge neutrality drives the ions thus expelling the plasma out of the critical region and producing a caviton localized in the density profile and steepening the profile in the vicinity of the ablation surface. In the process the resonance point is shifted deeper into the overdense region in close vicinity of the ablation surface. The high frequency electron-plasma waves are trapped in the density cavity and mutually enhance each other. Thus the cavitons serve as a resonant cavity for the high frequency fields. The trapped field together with the density caviton acts like a soliton. The solitons slowly move out of the resonance region and are regenerated. Consequently the absorption coefficient oscillates with a high frequency indicating a red shifted reflected wave which can be put to experimental varification. In addition large amplitude ion-waves are emitted in both directions from the resonance point which lead to rippling in transverse direction. Density rippling in the laser direction has also been observed in our experiments.

The phase velocity of the resonantly excited plasma waves is roughly proportional to $I^{0.33}$,

where L is the density scale length . Sharp density gradients due to steepening result in much lower phase velocity waves and lower velocity heated electrons. Essentially all the electrons are heated in contrast to the extensive suprathermal electrons produced by parametric instabilities close to the critical density. The heated electron distributions are close to exponential in velocity space. Moreover, since the plasma density in the superdense region is > $2n_c$ due to profile steepening; a larger number of particles participate in plasma heating to produce softer electron distribution, drastically suppressing the preheat which is so detrimental in laser-fusion scheme. The predominant non-linear force over the thermokinetic force essentially converts the optical laser energy directly into the directed mechanical energy of the plasma without heating it. Due to this directed mechanical energy thin blocks of plasma are accelerated to velocities $\sim 10^7$ cm/sec and implode the target without appreciable heating.

Carbon dixoide laser has been considered inefficient as a laser-fusion driver candidate for the following shortcomings: (1) CO_2 laser-plasma has relatively lower critical density $\sim 10^{19}$ cm^{-3} compared to 10^{21} cm^{-3} in Nd:glass laser plasmas. The classical absorption of laser light which is proportional to n_e^2 is therefore poor in CO_2 plasma. (2) The critical density surface in space is positioned far away from the ablation surface. The energy of the absorbed laser light at the critical density is therefore inefficiently transported to the ablation region. Although this aspect improves the ablation symmetry as the electrons transporting the energy from critical density surface to ablations surface are more uniformlay diffused. (3) Carbon dioxide is mainly absorbed by the process of linear mode conversion producing copious hot electrons which can preheat the pellet thwarting the compression.

However, at high laser intensities exceeding 10^{12} W/cm^2, the dominant non-linear force due to radiation pressure creates a shock plus front density profiles described by Max and Mckee[8]. Steepened

profiles thus produced shift the resonance point deeper in the vicinity of the ablation layer overcoming the short comings number 1 and 2 mentioned above. Fedosejevs et al[21] have demonstrated a peak density of 40 n_c in the over dense region close to ablation layer. The hot electrons produced initially by linear mode conversion would therefore be easily thermalised with cold overdense region and thus generate softer electron distribution overcoming the third mentioned short coming.

Chen and Liu[13] have shown that the absorption co-efficient due to radiation pressure is independent of laser wavelength and intensity as well as plasma temperature. The plasma acceleration produced by non-linear force of intense CO_2 laser is $\sim$ 10 times that produced by a Nd:glass laser[30]. Morever CO_2 laser efficiency is much higher than that of a Nd:glass laser.

Looking at these facts, carbon dioxide laser may be reconsidered as a fusion-driver candidate.

REFERENCES:

1. J.C.Adam, A.Gourdin Serveniere and G.Laval, Phys.Fluids,25, 376 (1982).
2. V.L.Ginzburg, Propagation of Electromagnetic waves in plasmas, Pergamon Press, New York (1964)
3. W.L.Kruer , Proc. IEEE, Minicourse on ICF, Montreal, Canada. (1979) Ed. C. Miley.
4. H.Hora, Phys. of Laser Driven Plasmas (John Wiley and Sons New York, 1981) p.129
5. V.Gapanov and M.A.Miller, Sov. Phys. JETP, 7, 168 (1958)
6. J.A.Stamper, Phys.Fluids, 18, 735 (1975)
7. F.F.Chen, Laser Plasmas and Laser Energy, Edited by H.Hora (Plenum Press, New York, 1975) p.317
8. C.E.Max and C.F.Mckee, Phys.Rev.Letttn, 39, 1336 (1977)
9. K.G.Estabrook, Phys.Fluids, 18, 1151 (1975)
10. K.Lee et al, Phys.Fluids, 20, 51 (1977)
11. J.Virmont, R.Pellat and A.Mora, Phys.Fluids 21, 567 (1978)

12. C.J.Morales and Y.C.Lee, Phys. Fluids, 20, 1135 (1977)
13. H.H.Chen and C.S.Liu, Phys.Rev.Letts, 18, 1147 (1977)
14. R.L.Stenzel, A.Y.Wong and H.C.Kim, Phys.Rev.Letts.,32, 654 (1974)
15. H.C.Kim, R.L.Stenzel and A.Y.Wong, Phys.Rev.Letts., 34, 886 (1974)
16. A.Y.Wong and R.L.Stenzel, Phy.Rev.Letts., 34, 727 (1975)
17. T.Tanikawa, A.Y.Wong and D.L.Eggleston, Phys. Fluids, 27, 1416 (1984)
18. A.Y.Wong, T.Tanikawa and A.Kythi, Phys.Rev.Letts., 58, 1375 (1987)
19. T.P.Donaldson and I.J.Spalding, Phys.Rev.Letts., 36, 467 (1976)
20. R.Fedosejevs et al, Phys.Rev.Letts., 39, 932 (1977)
21. R.Fedosejevs et al, Phys.Fluids, 24, 537 (1981)
22. Y.A.Zakharenkov et al. Sov.Phys.-JETP, 43, 283 (1976)
23. J.Briand et al, Phys.Fluids, 27, 2588 (1984)
24. H.Azechi et al, Phys.Rev.Letts, 39, 1144(1977)
25. D.T.Attwood et al, Phys.Rev.Letts., 40, 184 (1978)
26. A.Raven and O.Willi, Phys.Rev.Letts., 40, 184 (1978)
27. B.L.Henke et al, J.Opt Soc.Am., D1, 1540 (1986)
28. B.L.Henke et al, J.Opt.Soc.Am., B1, 828 (1984)
29. S.Sakabe, Phys. Rev.A, 26, 2159 (1982)
30. R.Dragila and J.Krepelka, Le J.De Physique, 39, 617 (1978)

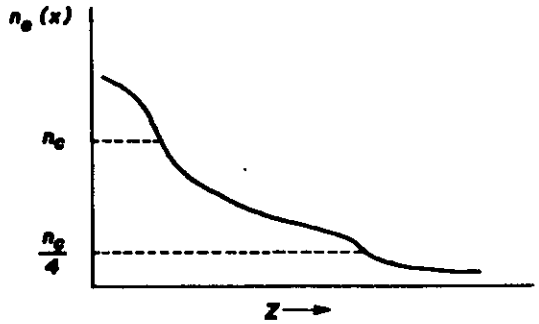

FIG. 1

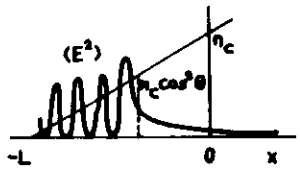

$\langle E^2 \rangle$ PROFILE FOR S-POLARIZATION

FIG. 2

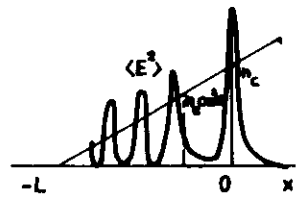

$\langle E^2 \rangle$ PROFILE FOR P-POLARIZATION

FIG. 3

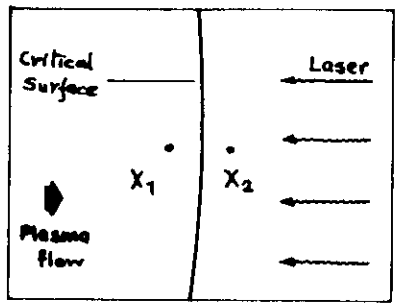

GEOMETRY FOR JUMP CONDITIONS

FIG . 4

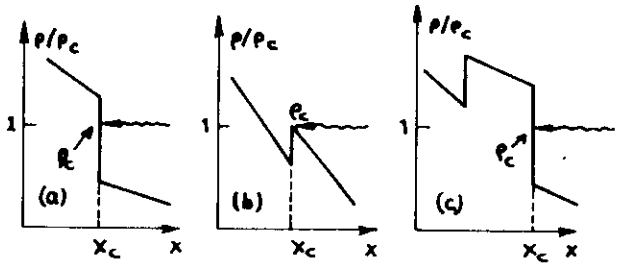

D-FRONT R-FRONT SHOCK D-FRONT

a b c

FIG. 5

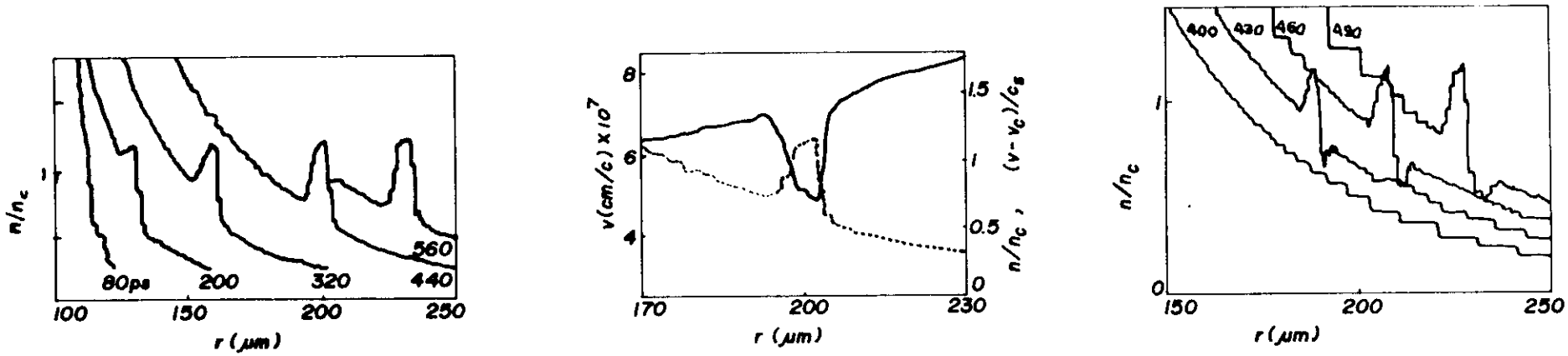
n/n_c
1
80ps
200
320
440
560
100
150
200
250
r (μm)
(a)
v(cm/c) x 10^7
8
6
4
1.5
1
0.5
0
n/n_c , (v - v_c)/c_s
170
200
230
r (μm)
(b)
400
430
460
490
n/n_c
1
0
150
200
250
r (μm)
(c)

FIG. 6

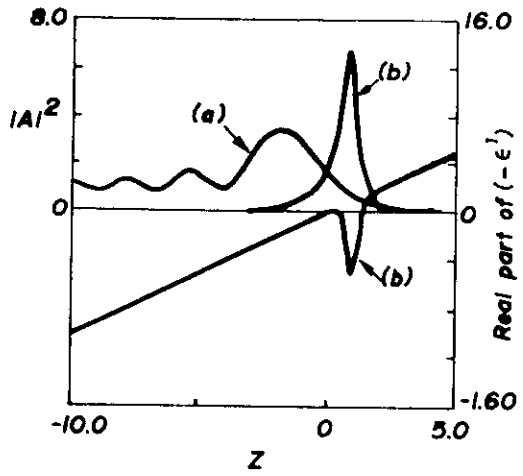
8.0
16.0
$|A|^2$
(a)
(b)
0
0
(b)
Real part of $(-\epsilon^1)$
-1.60
-10.0
0
5.0
Z

FIG. 7

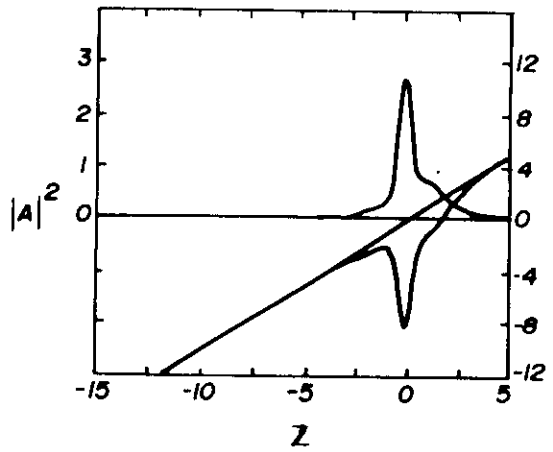
3
2
1
0
12
8
4
0
-4
-8
-12
$|A|^2$
-15
-10
-5
0
5
Z

FIG. 8

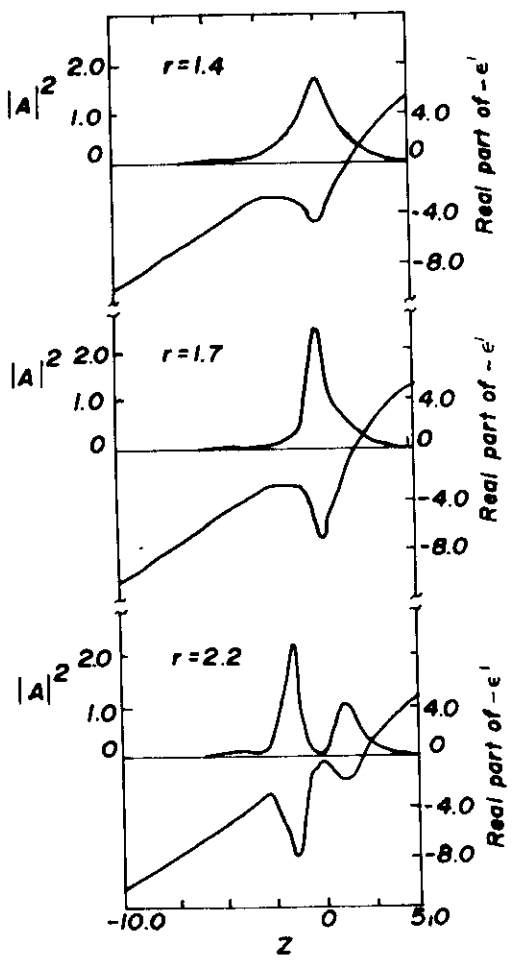
r=1.4
r=1.7
r=2.2
|A|²
2.0
1.0
0
4.0
0
-4.0
-8.0
Real part of -ε'
-10.0
0
5.0
Z

FIG. 9

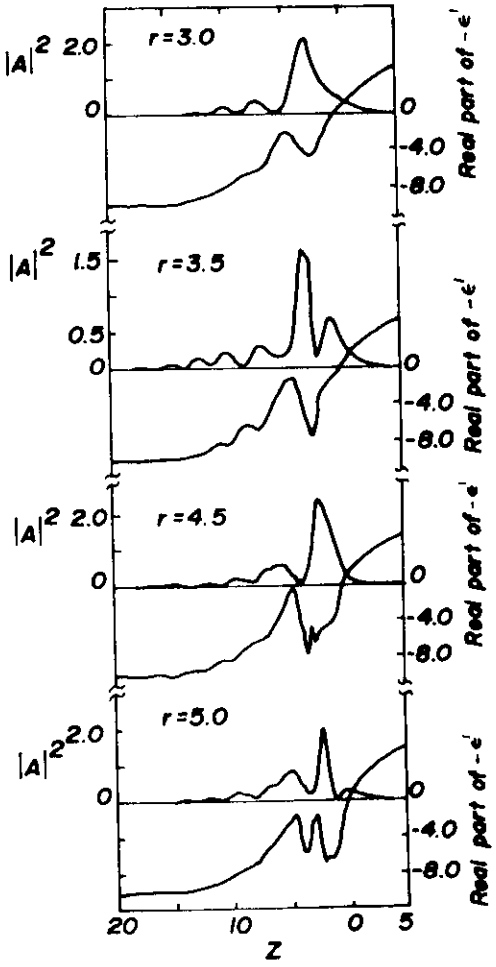
r=3.0
r=3.5
r=4.5
r=5.0
|A|²
2.0
1.5
0.5
0
-4.0
-8.0
Real part of -ε'
20
10
0
5
Z

FIG. 10

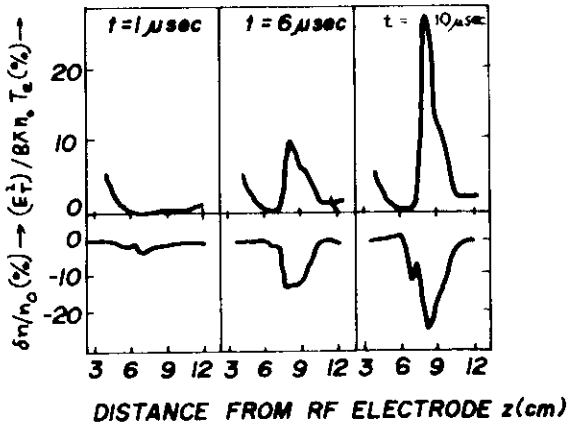
t = 1 μsec
t = 6 μsec
t = 10 μsec
20
10
0
0
-10
-20
3 6 9 12 3 6 9 12 3 6 9 12
DISTANCE FROM RF ELECTRODE z(cm)

FIG. 11

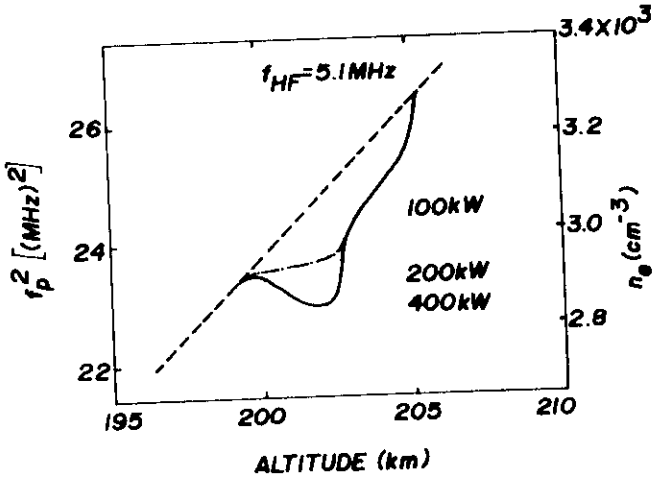

FIG. 12

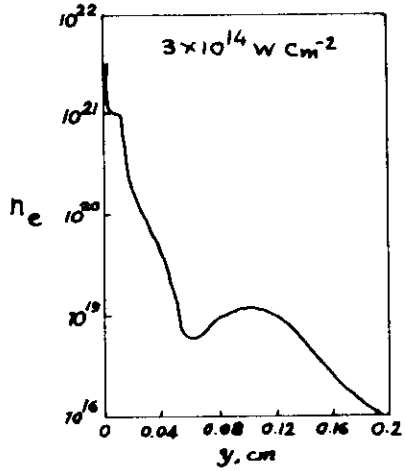
3×10^{14} W cm^{-2}
10^{22}
10^{21}
n_e
10^{20}
10^{19}
10^{16}
0
0.04
0.08
0.12
0.16
0.2
y, cm

FIG. 13

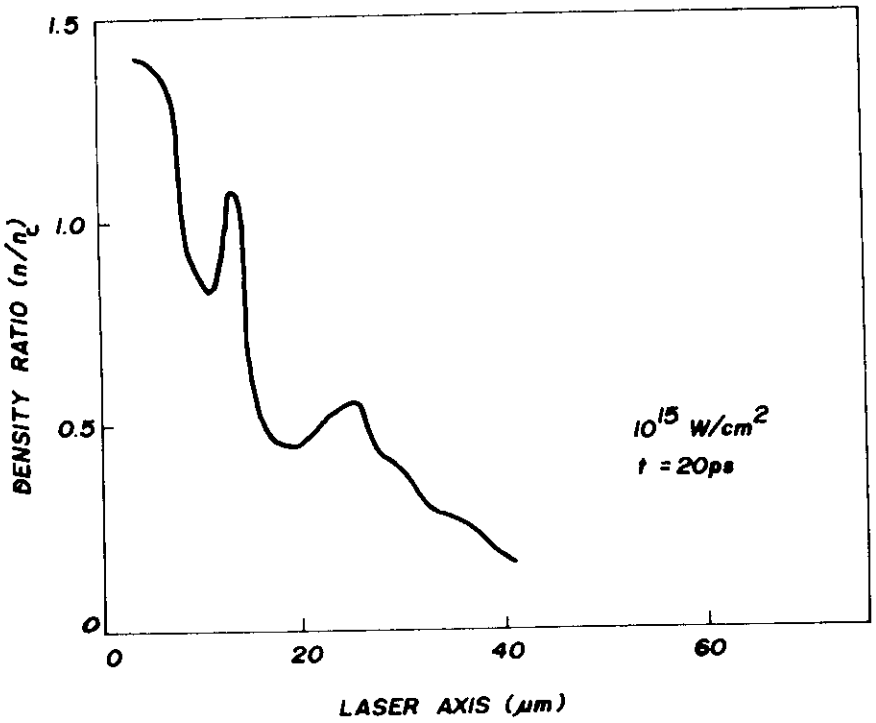
1.5
1.0
0.5
0
DENSITY RATIO (n/n_c)
10^15 W/cm^2
t = 20ps
0
20
40
60
LASER AXIS (μm)

FIG. 14

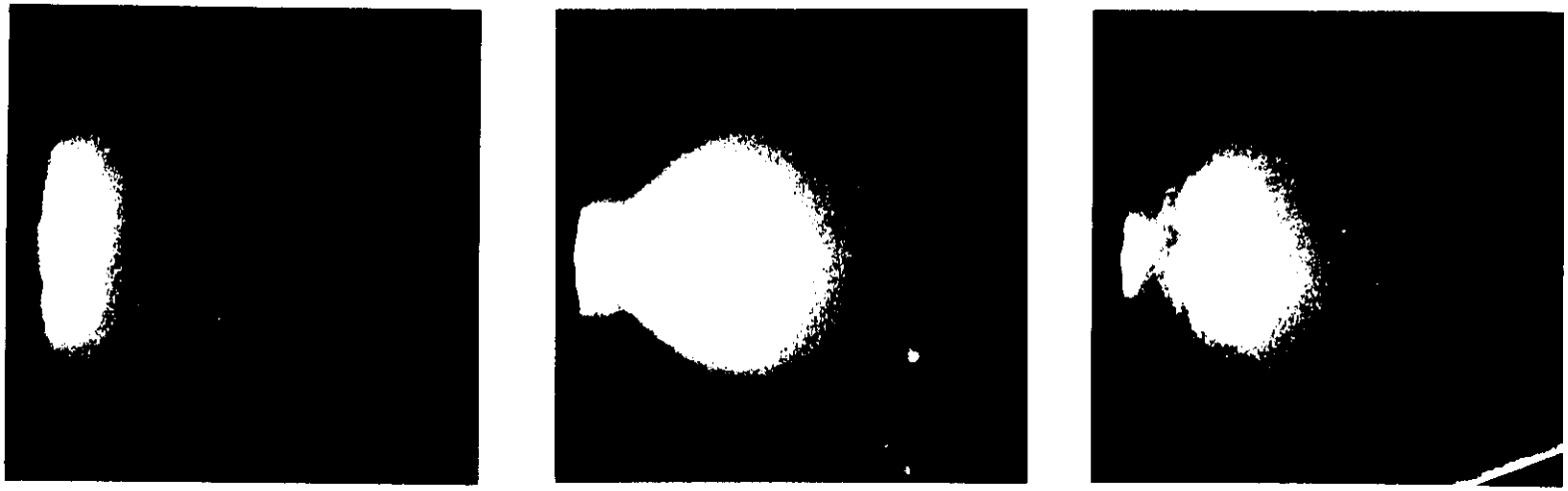

(a) 17.8 J (b) 19.6 J (c) 23.4 J

FIG. 15

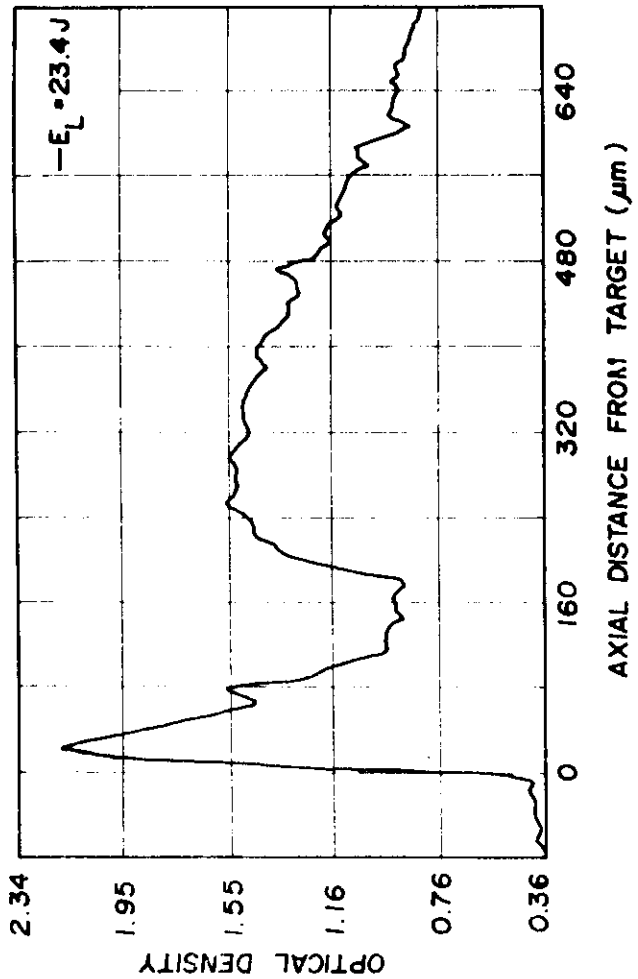

FIG. 16

ENERGY DENSITY PROFILES OF LASER PLASMA FROM PERSPEX SLAB TARGETS
LASER 1.06 MICRON, 17.8 J, 6 NS 30 MICRON FOCAL SPOT
LASER INTENSITY (4.2 X 10 ** 14 W / CM ** 2)

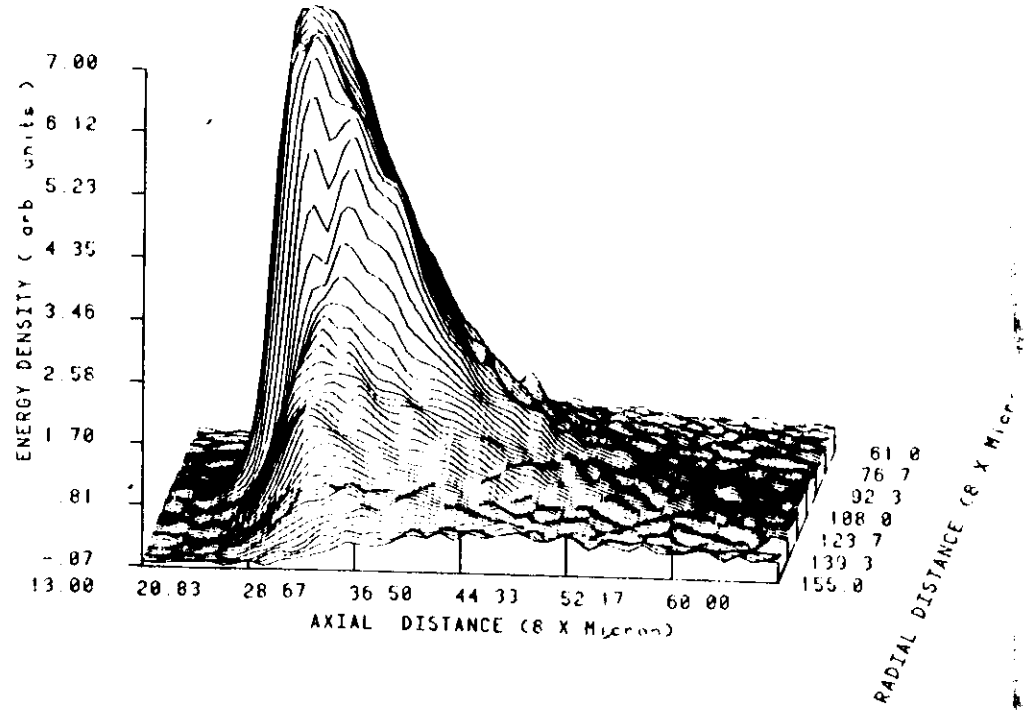

FIG. 17(a)

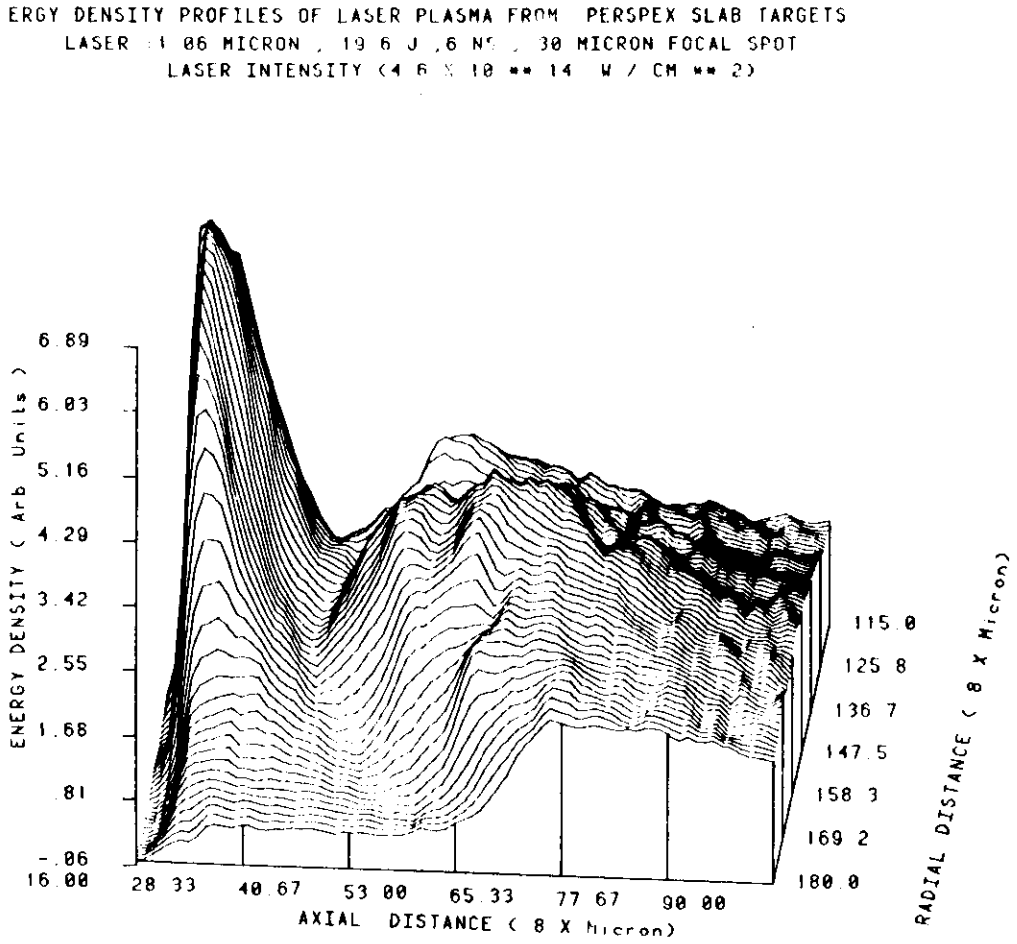

FIG. 17(b)

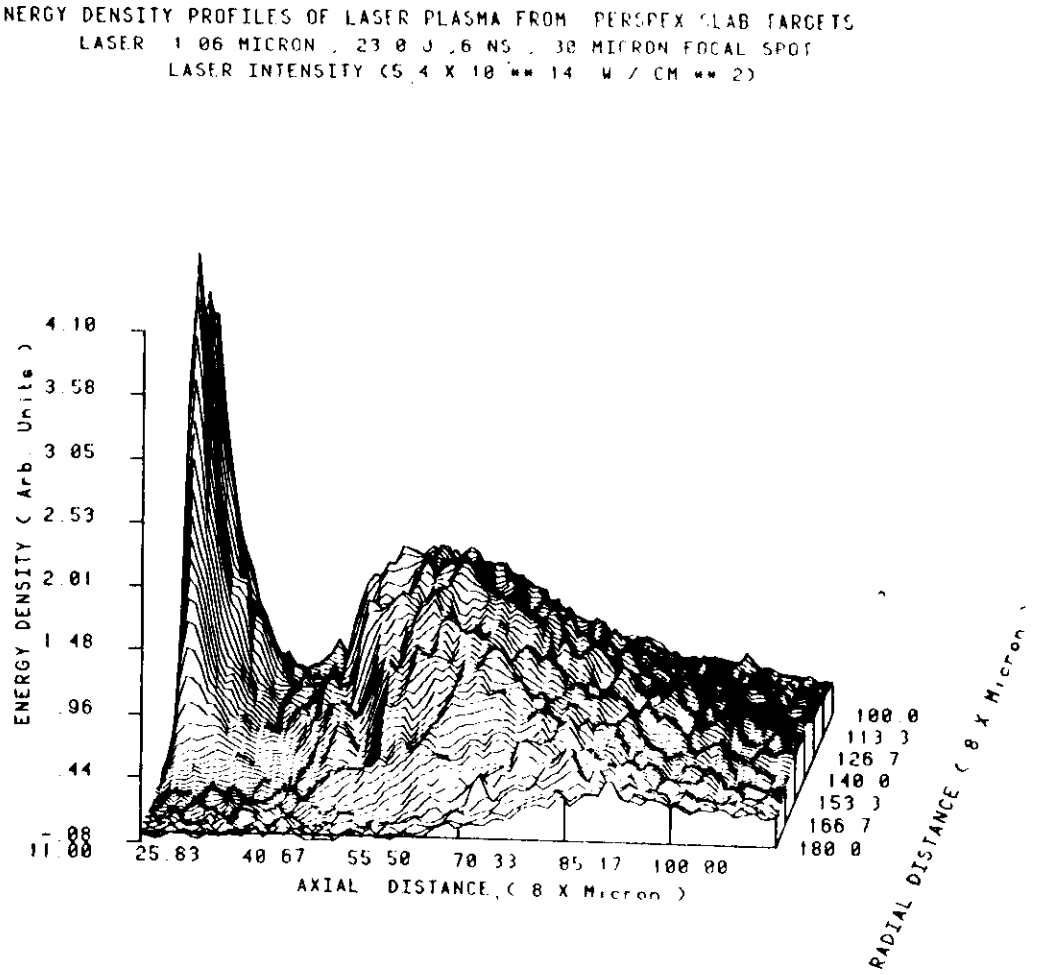

FIG. 17(c)

FIG. 17(d)

FIG. 18